Nonlinear Dyn (2007) 50:793–808
DOI 10.1007/s11071-007-9229-y

ORIGINAL ARTICLE

Contribution to efficiency of irreversible passive energy pumping with a strong nonlinear attachment

E. Gourdon · C. H. Lamarque · S. Pernot

Received: 10 January 2006 / Accepted: 20 June 2006 / Published online: 23 February 2007

Abstract The present study deals with nonlinear energy pumping which consists in passive irreversible transfer of energy from a linear structure to a nonlinear one. Various results (theoretical, numerical, and experimental) about energy pumping based on recent works are given. Thus, the phenomenon is studied for different excitations: transient and periodical. Moreover, advantages of such a system are carried out in particular efficiency of this phenomenon. That is why the robustness and comparison with classical tuned mass damper are analyzed. An application is considered with physical experiment using a reduced scale building.

Keywords Nonlinear energy pumping · Nonlinear normal modes · Reduced scaled building · Tuned mass damper

1 Introduction

The present study deals with energy pumping phenomenon which consists in passive irreversible transfer of energy from a linear system to a nonlinear attachment [1–3]. The aim is to be able to design efficient nonlinear energy sink devices (for example, with cubic nonlinearity [4, 5]), in particular, to attenuate modal responses for transient and steady vibrations. As analyzed in recent studies [1, 2], this energy transfer is closely related to nonlinear normal modes of undamped/unforced system and nonlinear resonance mechanism. It must be underlined that energy pumping phenomenon can be used to attenuate vibrations of a discrete or a continuous structure thanks to this nonlinear coupling. The present study differs from previous papers since here a strong nonlinear attachment is considered. Indeed, the energy pumping phenomenon has been widely studied [6, 7], but in the present study the essentially nonlinear coupling is used first of all to attenuate the vibrations during transient time. Energy pumping phenomenon is here the transient irreversible transfer of energy from a linear structure to a nonlinear structure [3]. Then, we study if this absorber (optimized for the transient time) can be efficient in stationary regime. Thus, the nonlinear attachment can be an efficient nonlinear vibration absorber as shown in [4], for example. The resonance which occurs is not a classical resonance between two linear systems. Indeed, the aim of energy pumping is far different since strong nonlinear attachment shall be designed to passively vibrate with any excited frequency. This way large motions can theoretically be reduced for more than one natural frequency by the same device. However, to be able to apply it in real practical applications, numerous numerical and analytical studies need to be done. As we will see, this kind of additional system has numerous advantages like a good robustness (if

E. Gourdon (✉) · C. H. Lamarque · S. Pernot
Ecole Nationale des Travaux Publics de l'Etat, LGM, URA CNRS 1652, Rue Maurice Audin, F-69518 Vaulx en Velin Cedex, France
e-mail: gourdon@entpe.fr

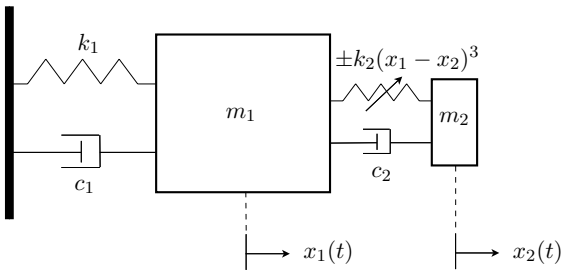

Fig. 1 The two-degree-of-freedom considered system

parameters are uncertain, then, it is possible to design attachment so that efficient energy pumping could be obtained) and can be better than a classical linear tuned mass damper (Frahm damper which is used in a lot of industrial structures) in terms of vibration control under periodical forcing. The structure of the paper is as follows. In the next section, energy pumping phenomenon with the capture of resonance is presented and the transient vibrations are studied. The robustness of the method is considered by using uncertain parameters to study the efficiency of energy pumping if parameters slightly vary. Then, the system with the nonlinear energy sink under periodical forcing is studied analytically with the multiple scale analysis and compared with complexification method. It allows to make comparison with the classical tuned mass damper. In Section 4, the above findings are tested and verified experimentally using appropriately designed reduced scale building with four floors. Section 5 contains conclusive remarks.

2 Energy pumping with transient vibrations: Robustness

A two-degree-of-freedom system composed of two weakly damped oscillators is considered as shown in Fig. 1. Here, x_1 and x_2 denote displacements of the main linear (or linearized) system and absorber, respectively. The following equations are obtained:

$$\begin{cases} m_1\dfrac{d^2x_1}{dt^2} + c_1\dfrac{dx_1}{dt} + k_1x_1 + c_2\left(\dfrac{dx_1}{dt} - \dfrac{dx_2}{dt}\right) \\ \quad +k_2(x_1 - x_2)^3 = 0, \\ m_2\dfrac{d^2x_2}{dt^2} + c_2\left(\dfrac{dx_2}{dt} - \dfrac{dx_1}{dt}\right) + k_2(x_2 - x_1)^3 = 0. \end{cases} \tag{1}$$

Nonlinear coupling is considered here. We should note that there is no linear force term in the second oscillator. Indeed, it is possible to consider only a pure nonlinear oscillator as it has been done in numerous studies [8, 9]. Moreover, this essential nonlinearity can be implemented practically as it has been done in [10, 11] where a pure cubic nonlinearity has been made physically with no linear force term. The linear primary structure is excited by an impulse, so we consider free oscillations of structures with initial conditions:

$$x_2(t=0) = x_1(t=0) = 0, \quad \frac{dx_2}{dt}(t=0) = 0,$$
$$\frac{dx_1}{dt}(t=0) = C_I. \tag{2}$$

Energy pumping phenomenon has been studied recently [12, 13] and it corresponds to a controlled one-way channeling of the vibrational energy to a passive nonlinear structure where it localizes and diminishes in time due to damping dissipation [1, 2]. Thus, through energy pumping, vibrations of a linear structure (subjected to an external excitation) can be attenuated thanks to a strongly nonlinear structure. This strong nonlinear attachment allows a 1:1 resonance responsible for the energy pumping phenomenon.

To observe this resonance capture which occurs, a time-frequency analysis must be performed since resonance between the linear mode and the nonlinear normal mode occurs during the transient responses. That is why we can use the Hilbert Transform (HT) and its properties which are often used in nonlinear free vibrations in nonstationary domain, in particular, the concept of Instantaneous Frequency (IF). As a generalization of the definition of frequency, IF is defined as the rate of change of the phase angle at time t of the analytic version of the signal [14]. Given a real signal $s(t)$, the analytic signal $z(t)$ is a complex signal having the actual signal as the real part and the Hilbert Transform of the signal as the imaginary component, namely:

$$z(t) = s(t) + jH[s(t)] = a(t)e^{j\phi(t)}, \tag{3}$$

where the amplitude $a(t)$ and the phase $\phi(t)$ are given by:

$$a(t) = \sqrt{(s(t))^2 + (H[s(t)])^2} \quad \text{and}$$
$$\phi(t) = \tan^{-1}\left(\frac{H[s(t)]}{s(t)}\right), \tag{4}$$

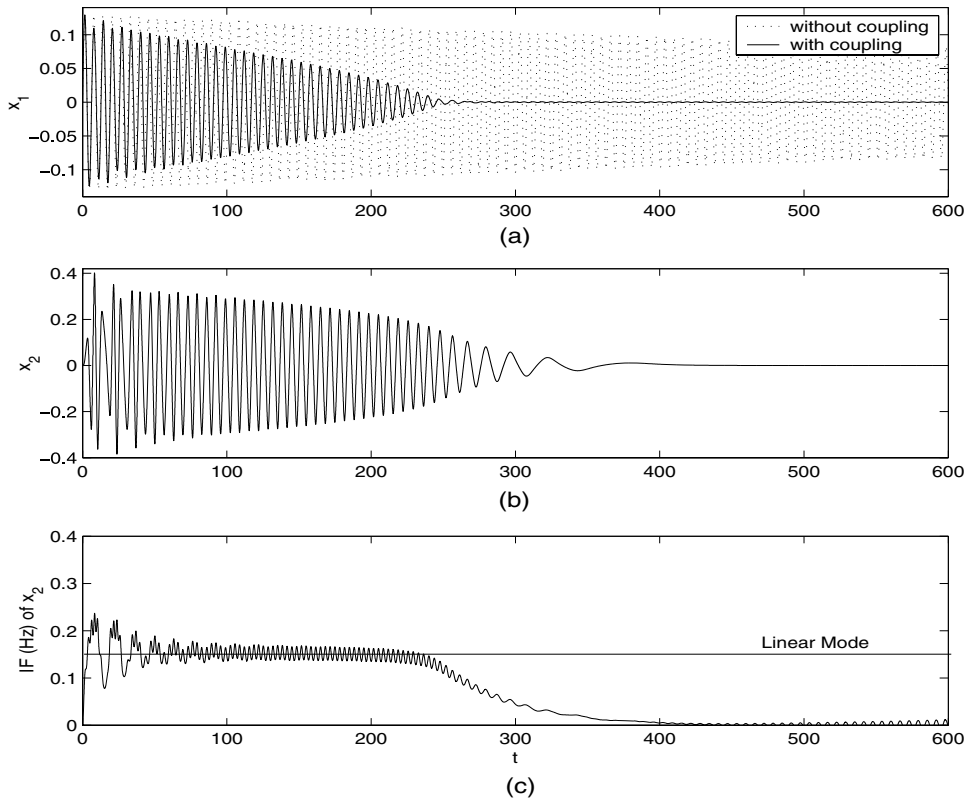

Fig. 2 Energy pumping phenomenon owing to a 1:1 resonance

and the Hilbert Transform is given by the principal value of the following integral:

$$H[s(t)] = \frac{1}{\pi}\int_{-\infty}^{\infty}\frac{s(\tau)}{t-\tau}d\tau. \tag{5}$$

The Instantaneous Frequency is defined by:

$$f_i(t) = \frac{1}{2\pi}\frac{d\phi(t)}{dt}. \tag{6}$$

The IF definition captures the time variation of the frequency accurately whereas when the Fourier domain is used, the results contain a large number of components with different frequencies and the simple nature of the signal is lost. Thus, a frequency analysis can be performed with the calculation of IF. Thus, as shown in Fig. 2 ($m_2/m_1 = 0.025$, $k_1/m_1 = 1$, $k_2/m_1 = 1$, $c_1/m_1 = 0.0015$, $c_2/m_1 = 0.0015$ and $C_I = 0.13$; the natural damping is very small to better "see" the phenomenon and the different resonances) the nonlinear attachment engages in nonlinear resonance. Clearly, when energy pumping occurs, it appears that a resonance capture occurs with the nonlinear oscillator: the instantaneous frequency of $x_2(t)$ becomes identical to the instantaneous frequency of the linear mode as shown in Fig. 2c (energy transfer occurs). As the energy of the attachment decreases due to damping, the attachment engages in 1:1 resonance during which targeted energy transfer from the linear structure to the nonlinear attachment occurs (attenuation of x_1 in Fig. 2). Moreover, as underlined in [15] and as shown in Fig. 2c, between 0 and 50s, a beating phenomenon seems to act as "trigger" for strong nonlinear energy transfers in the system under consideration, i.e., early beats (before $t = 50$ s) act as catalyzer for effective energy transfer (then, a 1:1 resonance between 50 and 250 s).

However, it is necessary to know if the method is efficient with uncertain parameters (i.e., to know if energy pumping still occurs when parameters are not well-known) to be able to apply it to real structures especially since damping (which is not well-known) plays a great role in the phenomenon. Since the nonlinear attachment will never perfectly reflect the design and also due to

problems of nonlinear identification, uncertainties also appear in the nonlinearity. To check those points, it is considered that the various parameters can be uncertain. That is why we can use a recent method which uses a projection on the basis of orthogonal polynomials to Gaussian variables [16]. One, then, proposes to extend and to use this method in the nonlinear case because the coefficients in front of the nonlinearities are not necessarily small so that the application of the perturbation method is difficult. Then, as shown in [17], the random parts of parameters noted $\tilde{\lambda}_j$ are rewritten in the form (with a Karhunen–Loeve expansion [18], for example):

$$\tilde{\lambda}_j = \sum_{k=1}^{n} \lambda_{jk} \xi_k, \tag{7}$$

where the ξ_k are independent Gaussian random variables with zero mean and unit variance and n is an expansion order. In our case, damping and nonlinear stiffness, for example, can be considered as uncertain (because damping is not well-known and we consider impulse responses for which damping is likely to play a great role. Moreover, because of the aging of the structure which modifies the parameters, the loosening of the nonlinearity can occur). x_1 and x_2 can be expanded in polynomial chaos series (on the basis of truncated polynomial chaos) involving the deterministic coefficients $x_{1i}(t)$ and $x_{2i}(t)$:

$$\begin{cases} x_1(t) = \sum_{i=0}^{N} x_{1i}(t) \Psi_i\left(\{\xi\}_{i=1}^{n}\right), \\ x_2(t) = \sum_{i=0}^{N} x_{2i}(t) \Psi_i\left(\{\xi\}_{i=1}^{n}\right), \end{cases} \tag{8}$$

where $\Psi_p(\xi) = \Psi_n(\xi_{i1}, \ldots, \xi_{ip})$ are multidimensional Hermite Polynomials [19] of degree p and ξ is the vector of p normal random variables $\{\xi_{i_k}\}_{k=1}^{p}$. The variables are multidimensional independent Gaussian random variables with zero mean and unit variance. The orthogonality relation of the generalized polynomial chaos takes the form:

$$\langle \Psi_i \Psi_j \rangle = \langle \Psi_i^2 \rangle \delta_{ij}, \tag{9}$$

where δ_{ij} is the Kronecker product in the Hilbert space of the random variables ξ and $\langle . , . \rangle$ is the inner product in the Hilbert space determined by the support of the Gaussian variables:

$$\langle f(\xi) g(\xi) \rangle = \int f(\xi) g(\xi) W(\xi) d\xi. \tag{10}$$

Here, $W(\xi)$ is the weighting function corresponding to the polynomial chaos basis $\{\Psi_i\}$. In the case of the Hermite polynomials, the weight function in the orthogonality relation (10) is:

$$W(\xi) = \frac{1}{\sqrt{(2\pi)^n}} e^{-\frac{1}{2}{}^t \xi \xi}, \tag{11}$$

where n is the dimension of ξ. For example, the one-dimensional ($n = 1, \xi = \xi_1$) Hermite polynomials are:

$$\Psi_0 = 1, \ \Psi_1 = \xi, \ \Psi_2 = \xi^2 - 1, \ \Psi_3 = \xi^3 - 3\xi \ldots \tag{12}$$

In our case, damping and nonlinear stiffness, for example, can be considered as uncertain. Let us expand c_1, c_2, k_2:

$$\begin{cases} c_1 = c_{1_0} + \sum_{k=1}^{n} c_{1_k} \xi_k, \\ c_2 = c_{2_0} + \sum_{k=1}^{n} c_{2_k} \xi_k, \\ k_2 = k_{2_0} + \sum_{l=1}^{n} k_{2_l} \xi_l, \end{cases} \tag{13}$$

where ξ_k, ξ_l are Gaussian random variables with zero mean and unit variance; c_{1_0}, c_{2_0}, and k_{2_0} represent the means; c_{1_k}, c_{2_k}, and k_{2_l} $(k, l = 1, \ldots, n)$ represent the coefficients in the Karhunen–Loeve expansion, for example. x_1 and x_2 are then replaced by their expansion in the equations, and the equations obtained are multiplied by Ψ_m for $m = 0, \ldots, N$. If the average is done (integration on the domain of the random variables) and by using the properties of orthogonality of the polynomials, a set of deterministic ordinary differential equations is obtained and must be solved. It is important to note that the values of $\langle \Psi_m^2 \rangle$, $\langle \Psi_i \Psi_j \Psi_k \Psi_m \rangle$, and $\langle \xi_k \Psi_i \Psi_m \rangle$ should be calculated only once (many values are null thanks to the properties of the polynomials), and be kept in memory for all calculations using this method. The formulation of the equations for $m = 0, \ldots, N$ leads to a system of $2(N + 1)$ deterministic ordinary differential equations. This system of equations can be easily solved

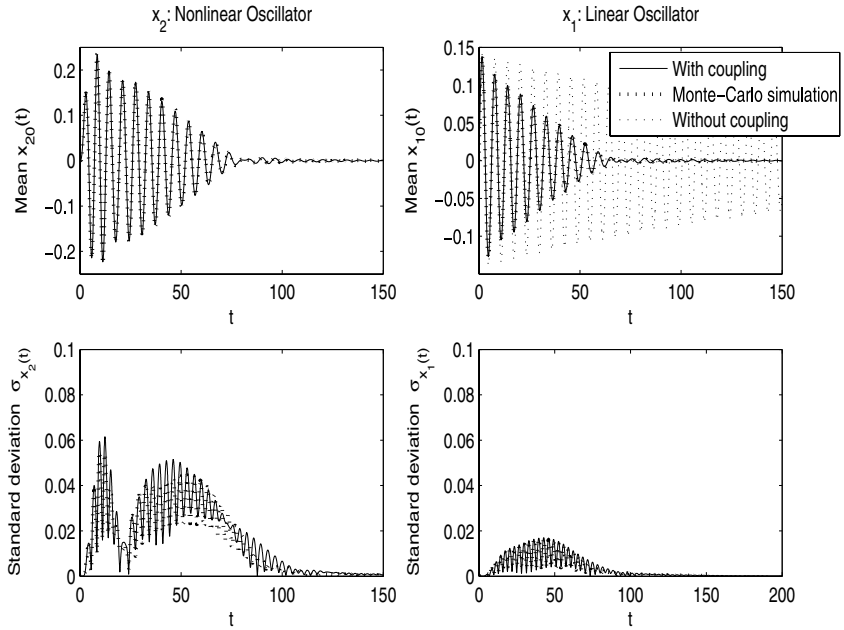

Fig. 3 Polynomial expansion of order 3 (*solid-line*): comparison with a Monte Carlo simulation (*dotted-line*)

using standard techniques for deterministic differential equations.

Once that the x_{i_m} are known, it is easy to find the mean and the variance of x_1 and x_2. Indeed,

- Means: $E(x_1) = x_{1_0}$ and $E(x_2) = x_{2_0}$,
- Standard deviations: $\sigma_{x_1} = \sqrt{\sum_{i=1}^{N} x_{1_i}^2 \langle \Psi_i^2 \rangle}$ and $\sigma_{x_2} = \sqrt{\sum_{i=1}^{N} x_{2_i}^2 \langle \Psi_i^2 \rangle}$.

This method is less time-consuming than Monte Carlo simulations and analytical results can be obtained as shown in [17]. Then, even if parameters are uncertain, it is possible to design attachment so that efficient energy pumping could be obtained as shown in Fig. 3 (mass ratio equals 5%) where the nonlinear stiffness is uncertain ($k_2 = k_{2_0} + \xi k_{2_1}$ with $k_{2_1} = 30\% k_{2_0}$). In this sense, the method allows to study robustness of energy pumping. As shown in this figure, chaos polynomial expansion is quite accurate compared to a Monte Carlo simulation and is far less time-consuming. The phenomenon of energy pumping still occurs when sufficient initial energy h is injected: attenuation of the linear oscillator and resonance of the nonlinear oscillator take place. This phenomenon of sufficient initial energy to have energy pumping in the deterministic case has been described in [1]. A chaos of order 2 or 3 is used because the approximation is quite good; the error compared to an "exact" solution is small (this point was underlined in [16] for linear equations). Indeed, to check that the projection on chaos polynomials is a good approximation of the random response, this method has been compared with a Monte Carlo simulation. This last method is more time-consuming and is only a numerical method but it provides "exact" results. Indeed, by using a chaos of order 3, a set of eight deterministic ordinary differential equations must be solved whereas by using 10,000 iterations of Monte Carlo (so that the Monte Carlo simulation converges very well), 2 deterministic ordinary differential equations (they are of the same type as the o.d.e. used with chaos of order 3) must be solved 10,000 times (so we have 10,000 o.d.e. to solve). By making the comparison between the responses of the previous system with previous parameters and a Monte Carlo simulation, a good concordance (even for the standard deviation) is observed as shown in Fig. 3 so chaos polynomials (even of order 2) are a good mean to obtain transient responses when uncertainties are introduced. Second, only damping of the nonlinear oscillator is considered as uncertain. By taking the same parameters as previously ($c_2 = c_{2_0} + \xi c_{2_1}$ with $c_{2_1} = 30\% c_{2_0}$), we can observe that energy pumping seems efficient for a large standard deviation as shown in the Fig. 4 where $p = 30\%$. By choosing a polynomial chaos expansion of order 2, the calculation of the mean and the standard

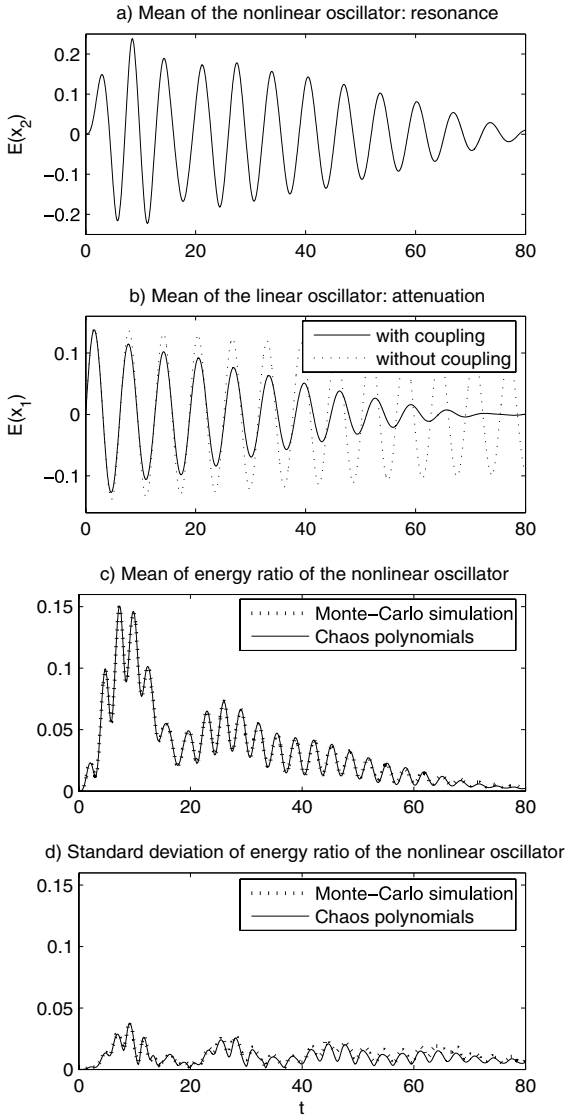

Fig. 4 Means and standard deviations of oscillators without and with coupling and energy ratio (mean and standard deviation) in the nonlinear oscillator using a chaos of order 2 and with c_2 uncertain

deviation of the energy ratio localized in the nonlinear added mass (where energies are calculated using the Hamiltonian of initial system without damping) shows (in Fig. 4c and d) that energy pumping occurs with a good efficiency when damping is uncertain since an important ratio of energy is quickly transferred to the additional structure in mean (the standard deviation is small). Various numerical investigations can be done and nonlinear normal modes (and the role of parameters) can also be analytically studied. Then, we can think of a future application (for example, the attenuation of building vibrations [4]) since the method seems to be efficient when the parameters slightly vary. In particular, it is possible to consider an experiment since, in practice, nonlinear parameters and damping are not necessarily well-known and can be determined experimentally with nonlinear identification (for example, the authors of [20] try to determine damping of buildings with experiments) with uncertainties. It remains to be said that this method allows to make further analytical calculation (we obtain after this method a set of deterministic equations which can be studied more precisely). Indeed, this method is interesting in terms of design since it will be possible to obtain analytical results (by studying the mean, the variance ,. . .), to make the inverse problem and to know exactly if the method will be robust.

3 Nonlinear energy sink with periodic forcing: Multiple scale analysis

The phenomenon is now considered with a periodic forcing:

$$\begin{cases} m_1\dfrac{d^2x_1}{dt^2} + c_1\dfrac{dx_1}{dt} + k_1x_1 + c_2\left(\dfrac{dx_1}{dt} - \dfrac{dx_2}{dt}\right) \\ \quad +k_2(x_1 - x_2)^3 = F\cos(\omega t), \\ m_2\dfrac{d^2x_2}{dt^2} + c_2\left(\dfrac{dx_2}{dt} - \dfrac{dx_1}{dt}\right) + k_2(x_2 - x_1)^3 = 0. \end{cases} \tag{14}$$

Owing to a multiple scale analysis, it is possible to plot the amplitude–frequency curve of the system analytically. The multiple scale method developed by [21] is a singular perturbation technique which may be used to solve nonlinear dynamical systems (some developments and applications can be seen in [22, 23]). Then, a dimensionless model is used: ($u = x_1$, $v = x_2 - x_1$)

$$\ddot{u} + \varepsilon\lambda_1\dot{u} + \omega_1^2u - \varepsilon\lambda_2\dot{v} - \varepsilon\omega_2^2v^3 = \varepsilon f\cos(\omega t), \tag{15}$$

$$\ddot{v} + (1+\varepsilon)\lambda_2\dot{v} - \varepsilon\lambda_1\dot{u} - \omega_1^2u + (1+\varepsilon)\omega_2^2v^3 = -\varepsilon f\cos(\omega t), \tag{16}$$

where

- $\varepsilon = \frac{m_2}{m_1}$: mass ratio,
- $\omega_1 = \sqrt{\frac{k_1}{m_1}}$: master structure inner frequency,
- $\omega_2 = \sqrt{\frac{k_2}{m_2}}$: coefficient of the nonlinearity,
- $\lambda_i = \frac{c_i}{m_2}$: damping factors $i = 1, 2$,
- $f = \frac{F}{m_1 \varepsilon}$: dimensionless forcing.

The solutions are sought with the following form:

$$u(t) = u_0(T_0,\ T_1) + \varepsilon u_1(T_0,\ T_1) + \cdots \tag{17}$$

$$v(t) = v_0(T_0,\ T_1) + \varepsilon v_1(T_0,\ T_1) + \cdots \tag{18}$$

with new independent times/derivative:

$$T_n = \varepsilon^n t, \quad n = 0, 1, \ldots$$

$$\frac{d}{d\,t} = D_0 + \varepsilon D_1 + \cdots = \frac{d}{d\,T_0} + \varepsilon \frac{d}{d\,T_1} + \cdots$$

Then, we are looking for a 1:1 resonance between the two oscillators (as shown by numerical simulations). Indeed, as shown in a lot of numerical evidences [3, 4] and analytical results[13, 24–27], when energy pumping occurs, u and v are oscillating with the same frequency. Here, it is a resonance with the same pulsation ω_1. It should be noted that it is not a classical resonance between two linear modes. Indeed, here the essential nonlinear system (with no linear term) can resonate with any linear frequency of the primary system. This point has been studied in numerous studies about this subject. However, in Equation (16) there are no terms in "$\omega_1^2 v$". That is why the term "$\omega_1^2 v$" is introduced into Equation (16). Thus, the system is now:

$$\begin{cases} \ddot{u} + \omega_1^2 u + \varepsilon\big(\lambda_1 \dot{u} - \lambda_2 \dot{v} - \omega_2^2 v^3 - f\cos(\omega t)\big) = 0, \\ \ddot{v} + \omega_1^2 v + \varepsilon\big((1+\delta)\lambda_2 \dot{v} - \lambda_1 \dot{u} - \delta\omega_1^2 u - \delta\omega_1^2 v \\ \quad + (1+\delta)\omega_2^2 v^3 + f\cos(\omega t)\big) = 0, \end{cases} \tag{19}$$

where $\delta = \varepsilon^{-1}$.

Then, multiple scales technique are used near 1:1 resonance: $\omega \equiv \omega_1 + \varepsilon\sigma$. So, stationary solutions

$$u_0 = a_0 \cos(\omega_1 T_0 + \sigma T_1 + c_0), \tag{20}$$

$$v_0 = b_0 \cos(\omega_1 T_0 + \sigma T_1 + d_0), \tag{21}$$

are introduced. So, in Equation (19), if the estimation presented in (20) and (21) is valid, one must adopt:

$$\delta\left[\lambda_2 \dot{v} - \omega_1^2 u - \omega_1^2 v + \omega_2^2 v^3\right] \sim O(1), \tag{22}$$

and, therefore, the expression in square brackets should be of order ε (but each term is not necessarily small). Indeed, as shown in a lot of numerical evidences [4, 24, 26] and analytical results [25, 28, 29], when energy pumping occurs, u and v are oscillating with the same frequency. Such a procedure is fully justified by detailed numerical analysis and by numerous previous papers. It is rather natural, as it describes slow modulation and damping of the vibrations with frequency close to $\frac{\omega_1}{2\pi}$. To verify it numerically, for example, we can take the following parameters (which will be used in the next numerical studies): $\varepsilon = 7.215\%$, $\omega_2 = 2000\,\mathrm{rad\,s^{-1}\,m^{-1}}$, $\omega_1 = 23.17\,\mathrm{rad\,s^{-1}}$, $\lambda_1 = 5.13\,\mathrm{s^{-1}}$, $\lambda_2 = 12\,\mathrm{s^{-1}}$, $m_1 = 1.677\,\mathrm{kg}$, $m_2 = 0.121\,\mathrm{kg}$, $\omega = 23.17\,\mathrm{rad\,s^{-1}}$ and $f = 1.5$. With those parameters, Fig. 5 shows the evolution of $(\lambda_2 \dot{v} - \omega_1^2 u - \omega_1^2 v + \omega_2^2 v^3)$ by numerical integration. This expression is of order $\varepsilon = 0.07215$, which verifies the hypothesis assumed previously. Moreover, the condition (22) restricts the kind of solutions which can be obtained by the multiscale method. However, the aim here is to study the mechanism of energy pumping underlined in numerous studies [3, 24, 25, 26, 28] which assume a 1:1 resonance at the pulsation ω_1. All other resonances which can occur in this kind of system are not studied in the present paper. This assumption has been checked explicitly by looking at the approximate solutions, both in multiscale and numerically as shown in Fig. 7.

So, stationary solutions are introduced in ε-scaled equations:

$$D_0 u_0 + \omega_1^2 u_0 = 0, \quad \varepsilon^0 \tag{23}$$

$$D_0 v_0 + \omega_1^2 v_0 = 0, \quad \varepsilon^0 \tag{24}$$

$$D_0^2 u_1 + 2D_0 D_1 u_0 + \lambda_1 D_0 u_0 - \lambda_2 D_0 v_0 + \omega_1^2 u_1 - \omega_2^2 v_0^3 = f\cos(\omega t), \quad \varepsilon^1 \tag{25}$$

$$D_0^2 v_1 + 2D_0 D_1 v_0 + (1+\delta)\lambda_2 D_0 v_0 - \lambda_1 D_0 u_0 + \omega_1^2 v_1 - \delta\omega_1^2 u_0 + (1+\delta)\omega_2^2 v_0^3 = -f\cos(\omega t), \quad \varepsilon^1 \tag{26}$$

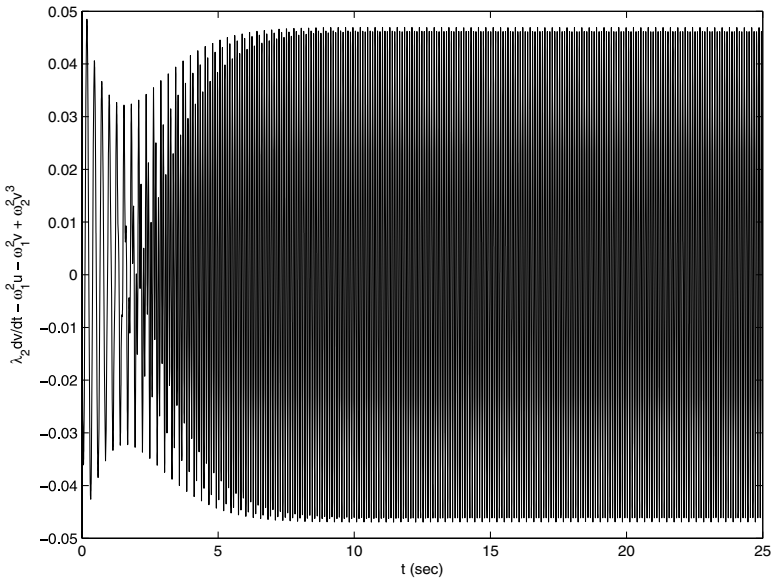

Fig. 5 Evolution of $(\lambda_2\dot{v} - \omega_1^2 u - \omega_1^2 v + \omega_2^2 v^3)$ by numerical integration ($\varepsilon = 0.07215$)

yielding eqs(u_1, v_1) involving $e^{j\omega_1 T_0}$, $e^{3j\omega_1 T_0}$ components. Cancelling secular parts in $e^{j\omega_1 T_0}$ gives resonant conditions for u_0, v_0. When all calculations are done, a_0, b_0, c_0, and d_0 are implicit solutions of the system:

$$a_0\omega_1\sigma - \frac{\lambda_2 b_0\omega_1 \sin(d_0 - c_0)}{2} + \frac{3\omega_2^2 b_0^3 \cos(d_0 - c_0)}{8} + \frac{f\cos(c_0)}{2} = 0, \tag{27}$$

$$\frac{\lambda_1 a_0\omega_1}{2} - \frac{\lambda_2 b_0\omega_1 \cos(d_0 - c_0)}{2} - \frac{3\omega_2^2 b_0^3 \sin(d_0 - c_0)}{8} + \frac{f\sin(c_0)}{2} = 0, \tag{28}$$

$$b_0\omega_1\sigma - \frac{\lambda_1 a_0\omega_1 \sin(c_0 - d_0)}{2} + \frac{\delta\omega_1^2 a_0 \cos(c_0 - d_0)}{2} + \frac{\delta\omega_1^2 b_0}{2} - \frac{3\omega_2^2 b_0^3(1+\delta)}{8} - \frac{f\cos(d_0)}{2} = 0, \tag{29}$$

$$\frac{(1+\delta)\lambda_2 b_0\omega_1}{2} - \frac{\lambda_1 a_0\omega_1 \cos(c_0 - d_0)}{2} - \frac{\delta\omega_1^2 a_0 \sin(c_0 - d_0)}{2} - \frac{f\sin(d_0)}{2} = 0. \tag{30}$$

A Newton procedure is then used to obtain the FrF of structure coupled with energy sink. As example, we consider $\varepsilon = 7.215\%$, $\omega_2 = 2700\,\mathrm{rad\,s^{-1}\,m^{-1}}$, $\omega_1 = 23.17\,\mathrm{rad\,s^{-1}}$, $\lambda_1 = 15\,\mathrm{s^{-1}}$, $\lambda_2 = 12\,\mathrm{s^{-1}}$, $m_1 = 1.677\,\mathrm{kg}$, $m_2 = 0.121\,\mathrm{kg}$ to plot the FrF of structures as shown in Fig. 6. Then, we should note that the assumption (22) and the fact that we are just looking at a resonance 1:1 (other kind of solutions which can be obtained by the multiscale analysis are not studied in the present paper) have been checked explicitly by

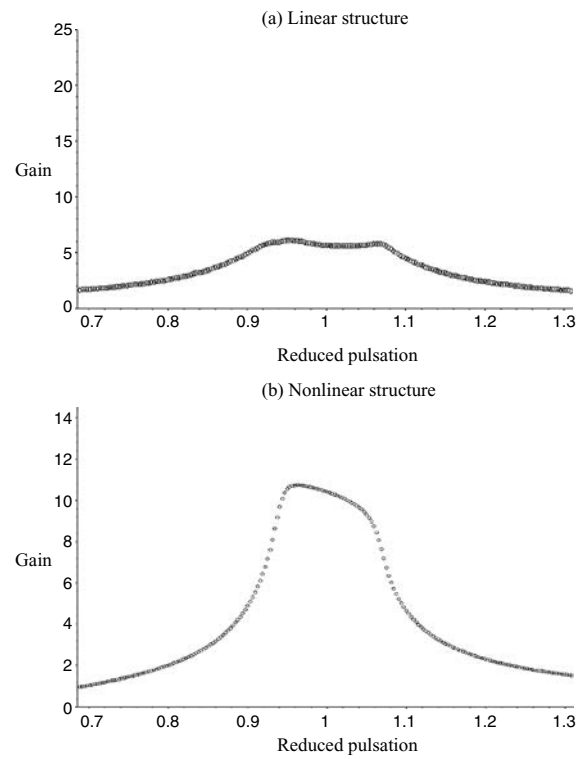

Fig. 6 FrF plotted owing to a multiple scale analysis

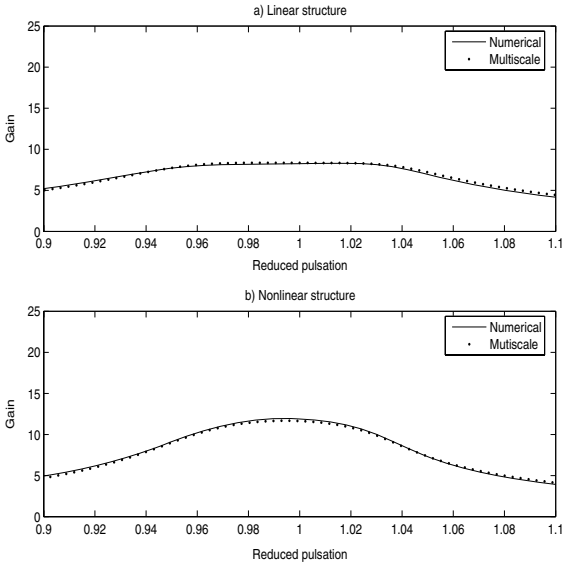

Fig. 7 Comparison between multiscale and numerical solutions

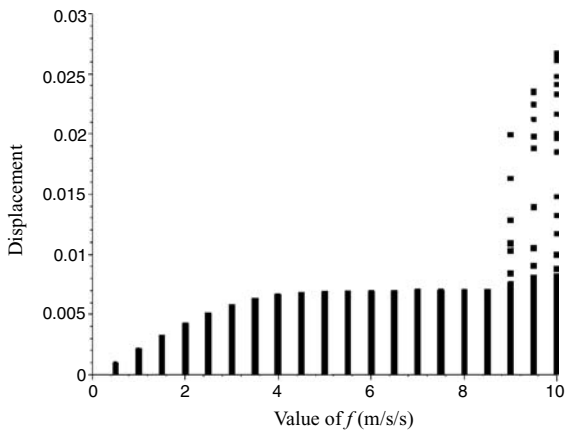

Fig. 8 Evolution of the FrF plotted owing to a multiple scale analysis

looking at the approximate solutions, both in multiscale and numerically as shown in Fig. 7 with the previous parameters (here, $f = 5$).

Moreover, by analyzing more precisely those FrF as shown in Fig. 8 ($\varepsilon = 7.215\%$, $\omega_2 = 3500\,\mathrm{rad\,s^{-1}\,m^{-1}}$, $\omega_1 = 23.17\,\mathrm{rad\,s^{-1}}$, $\lambda_1 = 5.13\,\mathrm{s^{-1}}$, $\lambda_2 = 12\,\mathrm{s^{-1}}$, $m_1 = 1.677\,\mathrm{kg}$, $m_2 = 0.121\,\mathrm{kg}$) where the amplitude of excitation f varies (this figure shows the maximum displacement of the primary structure versus the amplitude of the forcing f: for each value of f, the bar represents the interval of displacement of the primary structure; each point of the bar is for one fixed value of the external excitation ω so the top of the bar is the maximum value of displacement for one fixed value of f). In Fig. 7, we observe that for low amplitudes (before $f = 4$), energy pumping is not activated, for middle amplitudes, there exists an efficient range of sink device (the maximum displacement of the primary structure is not increasing when the amplitude f of the external forcing is increasing), and for large amplitudes (after $f = 9$), the phenomenon is weakly efficient. Moreover, to verify the good accuracy of the multiple scale analysis, we have compared the previous results with another method named complexification method which is similar to the technique developed in [30] (where the accuracy of the complexification method has been verified). Indeed, the considered system is governed by the following equations of motion (same system as previously):

$$\begin{cases} \ddot{x}_1 + \omega_1^2 x_1 + \varepsilon\lambda_1\dot{x}_1 + \varepsilon\lambda_2(\dot{x}_1 - \dot{x}_2) \\ \quad + \varepsilon\omega_2^2(x_1 - x_2)^3 = \varepsilon f\cos(\omega t), \\ \varepsilon\ddot{x}_2 + \varepsilon\lambda_2(\dot{x}_2 - \dot{x}_1) + \varepsilon\omega_2^2(x_2 - x_1)^3 = 0, \end{cases} \tag{31}$$

which can be rewritten as:

$$\begin{cases} \ddot{x}_1 + \omega_1^2 x_1 + + \varepsilon\lambda_1\dot{x}_1 + \varepsilon\lambda_2(\dot{x}_1 - \dot{x}_2) \\ \quad + \varepsilon\omega_2^2(x_1 - x_2)^3 - \varepsilon f\cos(\omega t) = 0, \\ \ddot{x}_2 + \lambda_2(\dot{x}_2 - \dot{x}_1) + \omega_2^2(x_2 - x_1)^3 = 0. \end{cases} \tag{32}$$

The complexification method described in [30] is used. Thus, the new complex variables

$$\psi_1 = \dot{x}_1 + j\omega x_1, \quad \psi_2 = \dot{x}_2 + j\omega x_2, \quad j^2 = -1, \tag{33}$$

are introduced. Then, the complex amplitudes are expressed as:

$$\psi_1 = \varphi_1 e^{j\omega t}, \quad \psi_2 = \varphi_2 e^{j\omega t}. \tag{34}$$

Substituting (33) and (34) into the equations of motion (32) and averaging at the excitation pulsation ω, we retain only terms containing $e^{j\omega t}$. We then obtain a set of two complex modulation equations governing the (slow) evolution of the complex amplitudes φ_i, $i = 1, 2$. To study steady state periodic solutions of the system, we impose stationary conditions to the modulation equations by setting $\dot{\varphi}_1 = \dot{\varphi}_2 = 0$. To

analyze the set of complex algebraic equations obtained (that governs the constant complex amplitudes of the two oscillators), we express the complex amplitudes in terms of their real and imaginary parts,

$$\varphi_1 = z_1 + jz_2, \quad \varphi_2 = z_3 + jz_4, \tag{35}$$

which upon substitution yield the following inhomogeneous set of four real equations:

$$\begin{cases} -\dfrac{\omega z_2}{2} + \dfrac{\varepsilon\lambda_1 z_1}{2} + \dfrac{\omega_1^2 z_2}{2\omega} + \dfrac{\varepsilon\lambda_2}{2}(z_1 - z_3) \\ \quad + \dfrac{3\varepsilon\omega_2^2}{8\omega^3}((z_1 - z_3)^2 + (z_2 - z_4)^2)(z_2 - z_4) = 0, \\ \dfrac{\omega z_1}{2} + \dfrac{\varepsilon\lambda_1 z_2}{2} + \dfrac{\varepsilon f}{2} - \dfrac{\omega_1^2 z_1}{2\omega} + \dfrac{\varepsilon\lambda_2(z_2 - z_4)}{2} \\ \quad - \dfrac{3\varepsilon\omega_2^2(z_1 - z_3)}{8\omega^3}((z_1 - z_3)^2 + (z_2 - z_4)^2) = 0, \\ -\dfrac{\omega z_4}{2} + \dfrac{\lambda_2}{2}(z_3 - z_1) + \dfrac{3\omega_2^2}{8\omega^3}((z_3 - z_1)^2 \\ \quad + (z_4 - z_2)^2)(z_4 - z_2) = 0, \\ \dfrac{\omega z_3}{2} + \dfrac{\lambda_2}{2}(z_4 - z_2) - \dfrac{3\omega_2^2}{8\omega^3}((z_3 - z_1)^2 \\ \quad + (z_4 - z_2)^2)(z_3 - z_1) = 0. \end{cases} \tag{36}$$

For fixed values of the system parameters, this set is numerically solved for varying pulsation ω to obtain the fundamental resonance curves of the system where the fast frequency of the steady-state response is identical to the frequency of the external excitation. The analytic approximations to the responses of the two oscillators are obtained by reserving the variable transformations, and are given by:

$$x_1(t) \approx \frac{|\varphi_1|}{\omega}\cos(\omega t + \phi_1),\ x_2(t) \approx \frac{|\varphi_2|}{\omega}\cos(\omega t + \phi_2), \tag{37}$$

where the amplitudes and phases are computed in terms of the solutions of the set (36) as follows,

$$|\varphi_1| = \sqrt{z_1^2 + z_2^2}, \quad |\varphi_2| = \sqrt{z_3^2 + z_4^2},$$
$$\phi_1 = \arctan\left(\frac{z_2}{z_1}\right), \quad \phi_2 = \arctan\left(\frac{z_4}{z_3}\right). \tag{38}$$

By taking the same values as previously ($\varepsilon = 7.215\%$, $\omega_2 = 4228\,\mathrm{rad\,s^{-1}\,m^{-1}}$, $\omega_1 = 23.17\,\mathrm{rad\,s^{-1}}$, $\lambda_1 = 5.13\,\mathrm{s^{-1}}$, $\lambda_2 = 12\,\mathrm{s^{-1}}$, $m_1 = 1.677\,\mathrm{kg}$, $m_2 = 0.121\,\mathrm{kg}$), we can see in Fig. 9 that the multiple scale analysis is in good agreement with the complexification method.

Moreover, for a periodical excitation and to better understand the interest of energy pumping compared to classical linear tuned mass damper, the amplitude–frequency curves (Fig. 10) can be compared. For example, two cases can be compared: (a) a primary structure with an optimal linear tuned mass damper (the

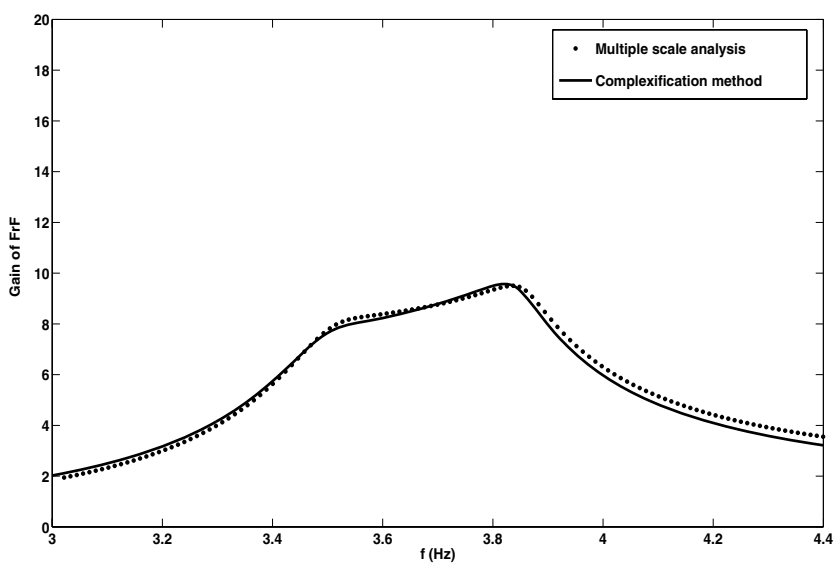

Fig. 9 Comparison between the complexification method and the multiple scale analysis

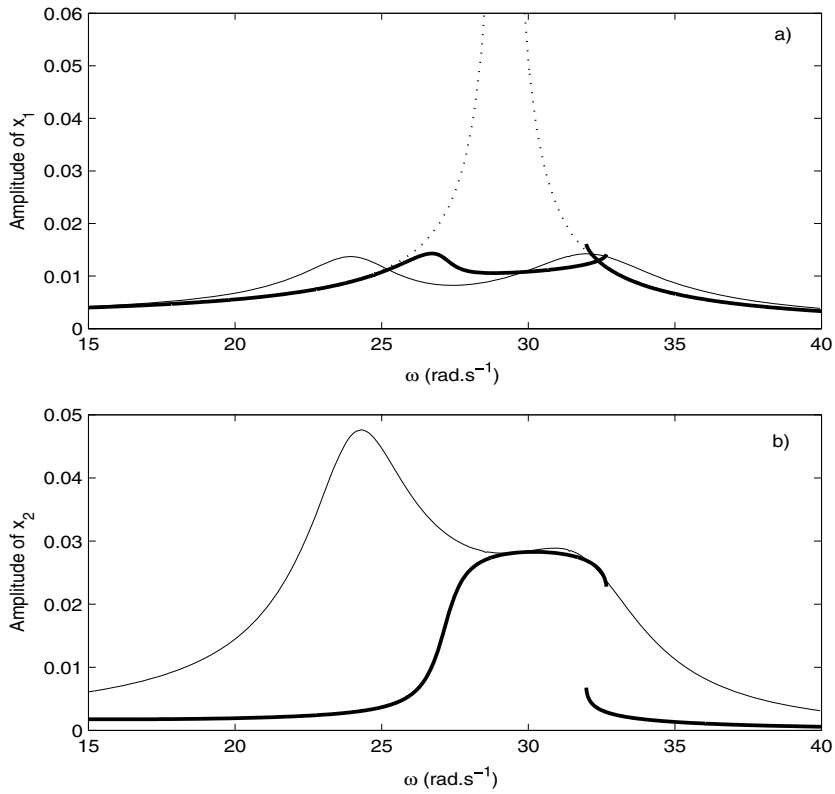

Fig. 10 Comparison with a Tuned Mass Damper (TMD) by calculating the stable stationary regimes. (a) Amplitude of $x_1(t)$, (b) Amplitude of $x_2(t)$. The *thick line* – denotes the amplitudes with the nonlinear coupling and the *thin line* – denotes the amplitudes with the linear TMD, the *dotted line* - - - denotes the amplitude of x_1 without coupling

optimization is described in [31]: $k_2 = 232.54\,\mathrm{N\,m^{-1}}$) (b) a primary structure with a nonlinear attachment $k_2/m_2 = 800{,}000$, $m_2/m_1 = 0.1$, $c_2/m_2 = 7$ (so, the specific natural damping in the nonlinear system is 0.39%). The damping coefficient and mass of the secondary added system are identical in both cases. Results are displayed in Fig. 10 for an harmonic excitation. The solutions for the nonlinear system have been calculated using the method described in [30]. We can clearly see an important advantage of the strong nonlinear coupling. Indeed, the curve with cubic coupling (i.e., the case in which the absorber is present) is always "under" (the amplitude is not amplified for a fixed value of forcing frequency $f = \omega/2\pi$) the curve without coupling (i.e., the case in which no absorber is present) which is not the case with a classical linear tuned mass damper where two resonances can appear. This last point can be dangerous for the structure, for example, with an earthquake where several frequencies can be excited and far from the main resonance the classical tuned mass damper can increase the vibrations. With strong cubic coupling, the features (in particular, the modes) of the system are not modified. Indeed, in Fig. 10, for $20 < \omega < 25$, the linear absorber is not effective and it is even dangerous for the primary structure. As shown in the Fig. 11, with a classical tuned mass damper and far from the main resonance two others peaks can appear. The advantages and disadvantages of the two kinds of absorbers (the TMD is the classical tuned mass damper and the NES is the strong nonlinear coupling with energy pumping phenomenon) can be summarized in Table 1 in which the disadvantages have been underlined.

So if the frequency of the linear primary structure is moving (because of aging...), one need to adjust the Frahm damper (Linear tuned mass damper) which is not the case with the NES.

4 Experimental verification

The experimental considered system is shown in Fig. 12. An experimental campaign is achieved on a small scaled four-storey building both to check feasibility and to investigate the energy pumping phenomenon on a realistic case-study. The four-storey building namely the linear master structure was manufactured

Table 1 Comparison of TMD and NES

Strongly nonlinear coupling	Linear tuned mass damper
Fitted to attenuate the whole frequency span of a mode	Fitted to attenuate a single frequency or narrow surrounding band
Reliable attenuation of natural frequency	Optimal attenuation of targeted frequency
Attenuation curve always remains underneath uncontrolled FrF	Possible amplification outside targeted frequency bandwidth
Little sensitive to frequency shifts FrF (structural damages, durability)	Sensitive to frequency shifts
Range of application	
Attenuation triggered beyond an amplitude threshold	Attenuation as soon as low forcing amplitude levels
Amplitude-dependent attenuation	Attenuation gain independent from excitation level
Free oscillations: yes / Steady vib.: yes	Free oscillations: yes / Steady vib.: yes
Transient vibrations: yes	Transient vibrations: no
Simultaneously control of several modes: cascades of resonances	No

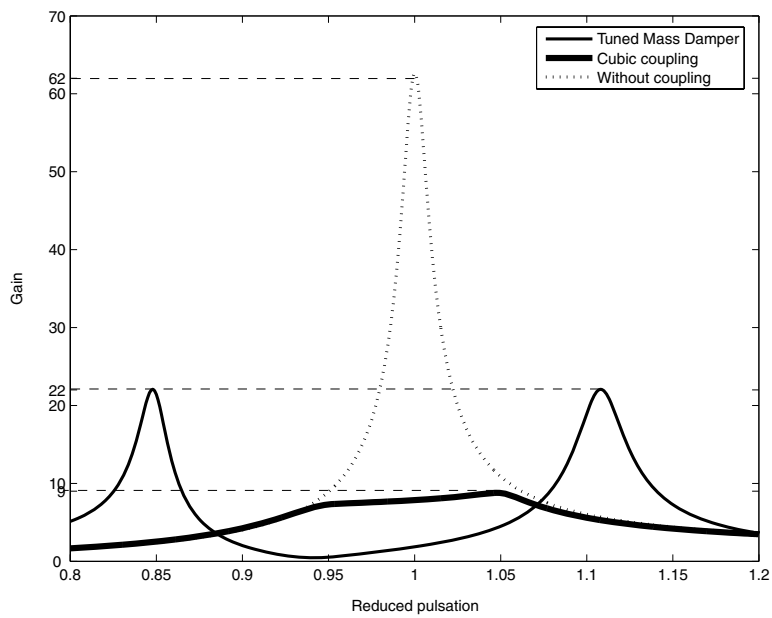

Fig. 11 Comparison with a classical linear tuned mass damper

by welding stainless steel columns and supporting beams. Steel plates were also welded on each storey to simulate realistic mixed steel–concrete slabs. The system is clamped on a plexiglass plate mounted on a shaking table driven by a Linmot electromagnetic linear motor. This latter is controlled by a Linmot E1000 MT controller which is characterized by the ability to efficiently stream almost any excitation profile (sine dwells, sine sweeps, random noise, pulses, earthquakes). Data acquisition of 6 PCB piezotronics accelerometers is performed by using a HP 3566A/67 Analyzer up to a sampling frequency of 12,800 Hz thus permitting to capture most instantaneous information of dynamic responses. The whole test rig is mounted on a heavy concrete block dynamically isolated from the ground. Linear eigenfrequencies and related specific damping of the main structure are identified when analyzing averaged FrF response curves obtained for random white noise or sine sweep excitations as illustrated in Fig. 13. Modal identification is performed by a pole-residual technique using Matlab structural dynamic toolbox SDtools. Generally speaking, eigenmodes are shear modes because of the low stiffness of the columns and high plates. As a result, accelerometers

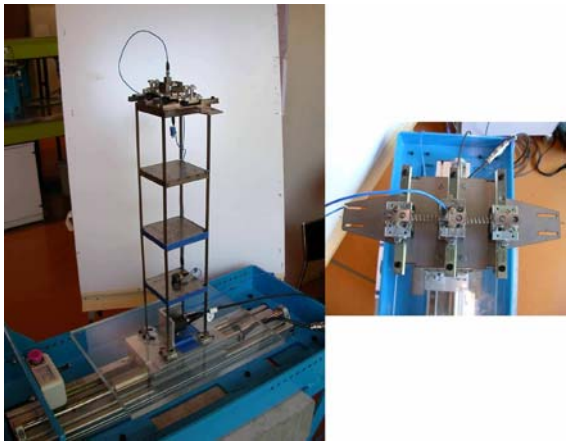

Fig. 12 Experimental system

placed on each storey of the structure indeed record actual horizontal components and not rotated ones. The secondary mass, of the absorber, can slide along a rail fixed to the top of the simple building. x_1 and x_2 represent, respectively, absolute displacements of the primary structure (at the top of the structure) and of the added mass. m_1 denotes the mass of the primary structure and m_2 the mass of the second added structure. In this experiment, the first modal idealized viscous damping coefficient between the primary mass and the support is c_1 and between the primary mass and the secondary mass is c_2. This model was designed, built, and tested at ENTPE. As underlined in [32], a cubic nonlinearity is made geometrically with two linear springs (k and l are the stiffness and length of each linear spring). However, when this spring is experimentally implemented, linear term appears since there exists a small prestress force in the spring. That is why even if the prestress force is kept to a minimum, linear coupling also appears. For the primary structure, we first consider only the first mode. An impulsion is considered at the top of the primary structure. Thus, the building and nonlinear absorber can be idealized by the model displayed in Fig. 1. The equations are similar to System (1) or (14) depending on the considered excitation. The experimental parameters are $m_2 = 0.121\,\text{kg}$, $m_1 = 1.677\,\text{kg}$. A modal analysis and experimental dynamic analysis of the structures give $k_1 = 900.3\,\text{N m}^{-1}$, $c_1 = 0.995\,\text{N s m}^{-1}$, $c_2 = 1.452\,\text{N s m}^{-1}$, and $k_2 = 1.48.10^6\,\text{N m}^{-3}$. The natural frequency of the linear oscillator is 3.69 Hz.

First of all, transient vibrations are analyzed. By considering an impulse at the first primary mass $x_2(t=0) = x_1(t=0) = 0$, $\frac{dx_2}{dt}(t=0) = 0$, $\frac{dx_1}{dt}(t=0) = 0.25$ with the help of a hammer (the load has been applied to the top floor of the model building (the representation of the primary structure by the building's first mode is thus reasonable)), then accelerations of free oscillations are measured and plotted as shown in Fig. 14 where energy pumping occurs (attenuation of the vibrations of the first mass owing to the resonance of the nonlinear one). The experimental results are in good agreement with the numerical integration of system (1) with the previous parameters (by taking

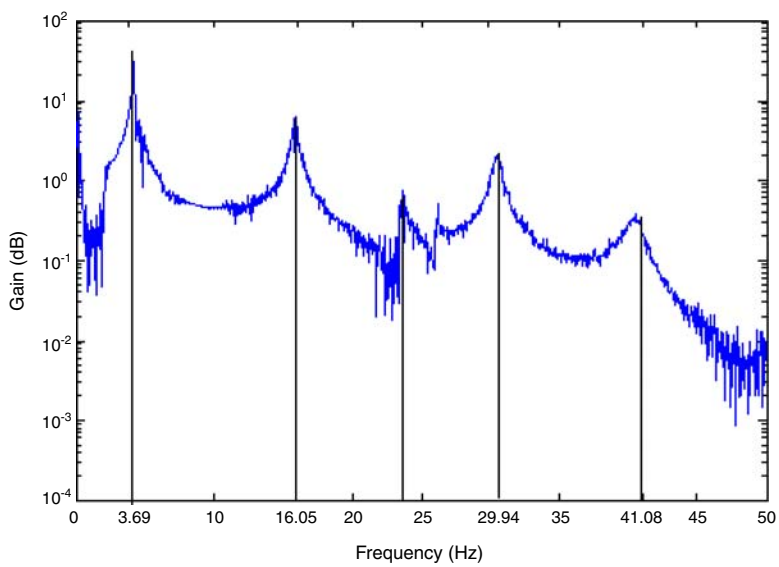

Fig. 13 Linear identification

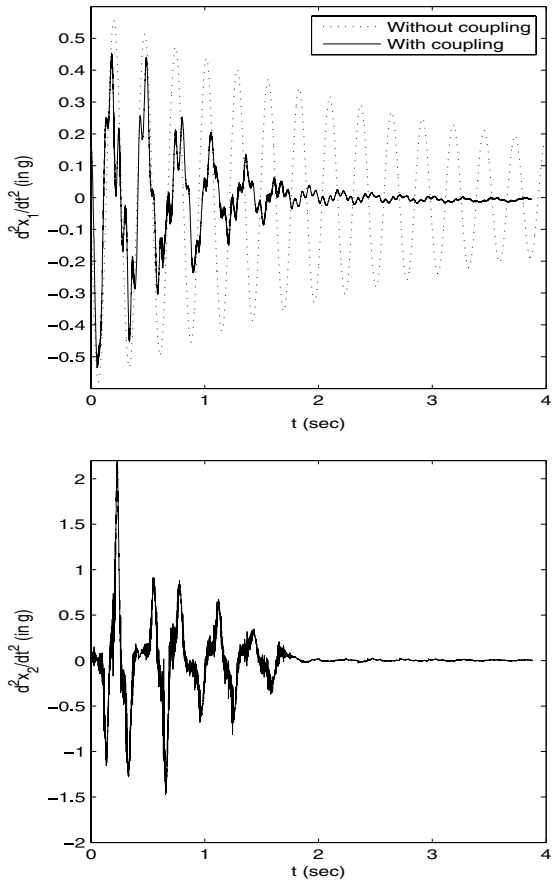

Fig. 14 Experimental results with an impulse

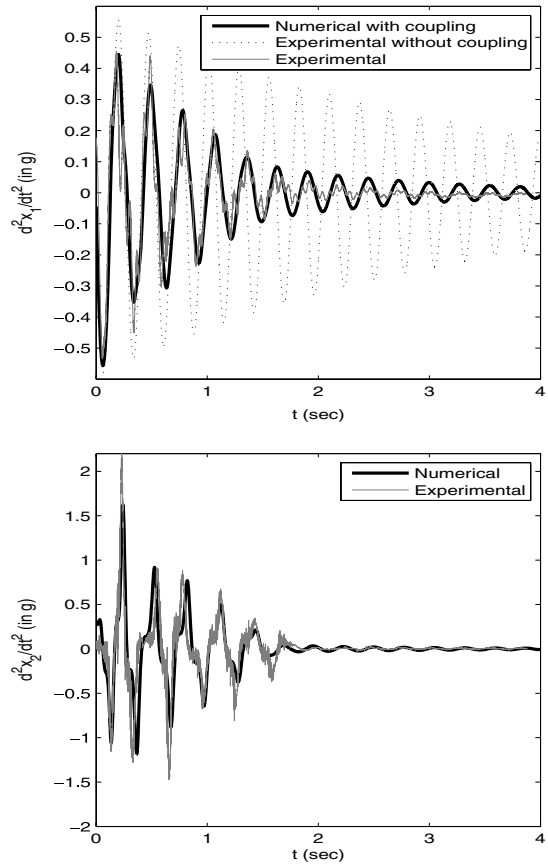

Fig. 15 Comparison of experimental and numerical results

only one mode into account in the numerical analysis) as shown in Fig. 15. We can clearly see that during energy pumping phenomenon, the first mode is only responsible for energy pumping. Indeed, by taking one mode into account in the theory (resonance with one mode) and in numerical simulations, the results are in good agreement with experimental results. There is just a small difference in experiment since the other modes change a little the response of x_1 but as underlined in [4], the first mode here is only responsible for energy pumping (there is resonance of the first mode but other modes are just oscillating with natural damping) and other modes of the linear structure are just simple damped oscillators. This is explained by the fact that the other modes of the structure (the second mode is 16.09 Hz) are very far from the main linear mode and the main resonance is at 3.69 Hz.

Then, when energy pumping occurs, it appears that a resonance capture occurs with the nonlinear oscillator as shown in Fig. 16 where the instantaneous frequency of experimental signal $x_2(t)$ (the experimental acceleration has been integrated twice with special filters) has been calculated with the Hilbert Transform. In Fig. 16, the instantaneous frequency of $x_2(t)$ becomes identical to the instantaneous frequency of the linear mode (3.69 Hz) (energy transfer occurs). Before $t = 2$s, the nonlinear normal mode is totally destroyed (brutal change of frequency of x_2) resulting in quasidestruction of vibrations.

Moreover, periodic forcing (owing to a small shaking table) can be studied. The experimental amplitude–frequency curves verify the theory seen in the previous part as shown in Fig. 17. Indeed, the curves with coupling (presence of the nonlinear absorber) are "under" the curve without coupling (there is no absorber) for different values of amplitude f so the main features of the main structure to be isolated are not modified. The NES appears to be very efficient.

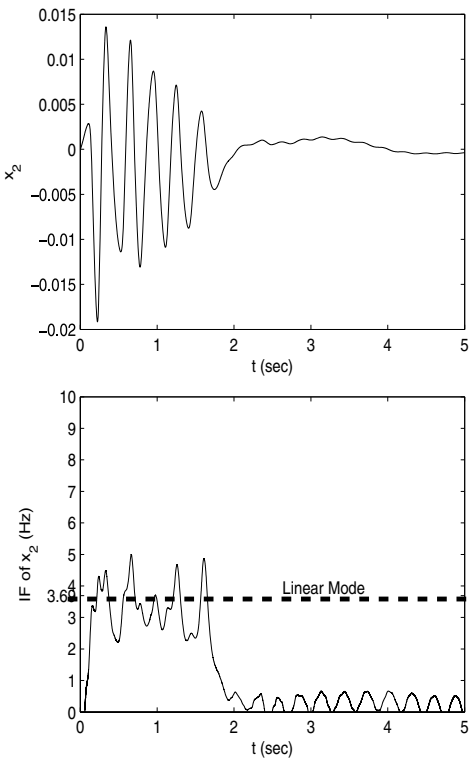

Fig. 16 Resonance capture phenomenon

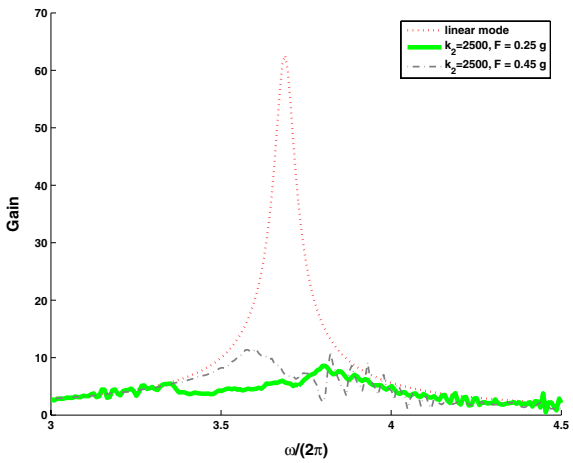

Fig. 17 Experimental results with a periodical excitation

5 Conclusion

Energy pumping phenomenon has been studied numerically, theoretically, and experimentally for different excitations. Not only is energy pumping efficient for transient vibrations, but it is also very efficient for periodic excitation. Indeed, experimental verification has shown the efficiency of energy pumping compared to classical linear tuned mass damper. Not only is the phenomenon robust theoretically as shown in the first part, but it is possible to implement it practically with a small realistic building model. Moreover, this study has shown advantages of using this kind of absorber instead of using classical tuned mass damper. This main point is the strong nonlinear coupling. Indeed, weakly linear (or weakly nonlinear) tuned mass dampers are commonly used to absorb the vibrations of a specific linear mode of a structure and its design is often optimized to widen the resonant frequency range. The tuned mass damper is adjusted to fit a natural frequency of the structure and the weak nonlinearity only slightly enlarges the efficient frequency span. Energy of the tuned mass damper is dissipated by a damper element. They are not very useful if one considers frequency shifts resulting from structural damages or durability problems. Although designed to absorb harmonic resonant excitations, the efficiency of the classical tuned mass dampers meets severe drawbacks when excitations are transient waves. The aim of energy pumping is far different since strong nonlinear attachment shall be designed to passively vibrate with any excited frequency. This way large motions can theoretically be reduced for more than one natural frequency by the same device. Cascades of resonance capture may even occur meaning that the energy sink is able to pass from one mode to another while extracting energy from them. Contrary to the case of standard tuned mass dampers, energy transfer is irreversible because of modal localization which prevents the energy from being released back to the main structure. It remains to consider the implementation of such a system in real buildings.

References

1. Gendelman, O., Manevitch, L.I., Vakakis, A.F., Closkey, R.M.: Energy pumping in nonlinear mechanical oscillators: Part I – dynamics of the underlying Hamiltonian systems. J. Appl. Mech. **68**, 34–41 (2001)
2. Vakakis, A.F., Gendelman, O.: Energy pumping in nonlinear mechanical oscillators: Part II – resonance capture. J. Appl. Mech. **68**, 42–48 (2001)
3. Manevitch, L.I., Gendelman, O., Moussienko, A.I., Vakakis, A.F., Bergman, L.: Dynamic interaction of a semi-infinite linear chain of coupled oscillators with a strongly nonlinear end attachment. Physica D **178**, 1–18 (2003)
4. Gourdon, E., Lamarque, C.H.: Energy pumping with various nonlinear structures: numerical evidences. Nonlinear Dyn. **40**, 281–307 (2005)

5. Gourdon, E., Lamarque, C.H.: Energy pumping for a larger span of energy. J. Sound Vib. **285**, 711–720 (2005)
6. Tondl, A., Nabergoj, R.: Dynamic absorbers for an externally excited pendulum. J. Sound Vib. **234**(4), 611–624 (2000)
7. Tondl, A.: Vibration quenching of an externally excited system by means of a dynamic absorber. Acta Techn. CSAV **43**, 301–309 (1998)
8. McFarland, D.M., Bergman, L., Vakakis, A.F., Manevitch, L.I., Gendelman, O.: Energy pumping into passive nonlinear energy sinks attached to forced linear substructures: analytical and experimental results. In: Ninth Conference on Nonlinear Vibrations, Stability, and Dynamics of Structures, Session 3, Virginia Polytechnic Institute and State University, Blacksburg, VA (2002)
9. Gendelman, O., Manevitch, L.I., Vakakis, A.F., Bergman, L.: A degenerate bifurcation structure in the dynamics of coupled oscillators with essential stiffness nonlinearities. Nonlinear Dyn. **33**(1), 1–10 (2003)
10. McFarland, D.M., Gipson, D.L., Vakakis, A.F., Bergman, L.: Characterization of an essentially nonlinear 2-DOF vibration test apparatus. In: Proceedings of the 15th ASCE Engineering Mechanics Conference, Columbia University, New York, 2–5 June, 1–8 (2002)
11. McFarland, D.M., Vakakis, A.F., Bergman, L.: Experimental verification of the performance of a nonlinear energy sink. In: Proceedings of the 15th ASCE Engineering Mechanics Conference, Columbia University, New York, 2–5 June (2002)
12. Vakakis, A.F., Kounadis, A.N., Raftoyiannis, I.G.: Use of nonlinear localization for isolating structures from earthquake-induced motions. Earthq. Eng. Struct. Dyn. **28**, 21–36 (1999)
13. Vakakis, A.F., Manevitch, L.I., Gendelman, O., Bergman, L.: Dynamics of linear discrete systems connected to local, essentially non-linear attachments. J. Sound Vib. **264**, 559–577 (2003)
14. Ville, J.: Théorie et application de la notion de signal analytique. Cables Transm. **2A**(1), 61–74 (1948)
15. Lee, Y.S., Kershen, G., Vakakis, A.F., Panagopoulos, D.M., Bergman, L.A., McFarland, D.M.: Complicated dynamics of a linear oscillator with a light, essentially nonlinear attachment. Physica D **204**(1–2), 41–69 (2005)
16. Dessombz, O.: Analyse dynamique de structures comportant des parametres incertains. Ph.D. Thesis, Ecole Centrale de Lyon, Lyon, France, 2000-36 (2000)
17. Gourdon, E., Lamarque, C.H.: Nonlinear Energy Sink with Uncertain Parameters. J. Comput. Nonlinear Dyn. **1**(3), 187–195 (2006)
18. Loeve, M.: Probability Theory, 4th edn. Springer-Verlag, Berlin (1977)
19. Xiu, D., Karniadakis, G.E.: The Wiener-Askey polynomial chaos for stochastic differential equations. SIAM J. Sci. Comput. **24**(2), 619–644 (2002)
20. Boutin, C., Ibraim, E., Hans, S.: Auscultation de bâtiments réels en vue de l'estimation de la vulnérabilité. Veme Colloque National AFPS, Cachan, pp. 298–305 (1999)
21. Nayfeh, A.H.: Perturbation Methods. Wiley-Interscience, New York (1973)
22. Nayfeh, A.H., Mook, D.T.: Nonlinear Oscillations. Wiley-Interscience, New York (1979)
23. Nayfeh, J.A.: A perturbation method for treating nonlinear oscillation problems. J. Math. Phys. **XLIV**, 368–374 (1965)
24. Gendelman, O.V., Gorlov, D.V., Manevitch, L.I., Moussienko, A.I.: Dynamics of coupled linear and essentially nonlinear oscilliator with substantially different masses. J. Sound Vib. **286**(1–2), 1–19 (2005)
25. Gendelman, O.V.: Bifurcations of nonlinear normal modes of linear oscillator with strongly nonlinear damped attachment. Nonlinear Dyn. **37**(2), 115–128 (2004)
26. Vakakis, A.F., Manevitch, L.I., Mikhlin, Yu.V., Pilipchuk, V.N., Zevin, A.A.: Normal Modes and Localization in Nonlinear Systems. Wiley Interscience, New York (1996)
27. Vakakis, A.F.: Inducing passive nonlinear energy sinks in vibrating systems. ASME J. Vib. Acoust. **123**(3), 324–332 (2001)
28. Gendelman, O.V., Gourdon, E., Lamarque, C.H.: Quasiperiodic energy pumping in coupled oscillators under periodic forcing. J. Sound Vib. **294**, 651–662 (2006)
29. Gendelman, O.V., Starosvetsky, Y.: Quasiperiodic response regimes of linear oscillator coupled of nonlinear energy sink under periodic forcing. J. Appl. Mech., in press (2006)
30. Jiang, X., McFarland, D.M., Bergman, L.A., Vakakis, A.F.: Steady state passive nonlinear energy pumping in coupled oscillators: Theoretical and experimental results. Nonlinear Dyn. **33**, 87–102 (2003)
31. Den Hartog, J.P.: Mechanical Vibration. McGraw-Hill, New York (1947)
32. McFarland, D.M., Bergman, L., Vakakis, A.F.: Experimental study of non-linear energy pumping occurring at a single fast frequency. Int. J. Non-Linear Mech. **40**, 891–899 (2005)